Journal of Alloys and Compounds 1010 (2025) 177828

Contents lists available at ScienceDirect

Journal of Alloys and Compounds

journal homepage: www.elsevier.com/locate/jalcom

$Co_3Ga_2Ge_5$: Probing site mixing of the Ru_3Sn_7 structure type with elements difficult to distinguish by diffraction

W. Kice Brown [a], Ifeoluwa P. Oyekunle [b], Erica Truong [b], Yudan Chen [b], Bright Ogbolu [b], Benny Schundelmier [c,d], Shaun O'Donnell [e], Rebecca W. Smaha [e], Yan-Yan Hu [b,d], Kaya Wei [d], Gregory T. McCandless [a], Julia Y. Chan [a,*]

[a] Department of Chemistry and Biochemistry, Baylor University, Waco, TX 76706, United States
[b] Department of Chemistry and Biochemistry, Florida State University, Tallahassee, FL 32306, United States
[c] Department of Physics, Florida State University, Tallahassee, FL 32306, United States
[d] National High Magnetic Field Laboratory, Florida State University, Tallahassee, FL 32310, United States
[e] Materials Science Center, National Renewable Energy Laboratory, Golden, CO 80401, United States

ARTICLE INFO

Keywords:
Intermetallics
Co-Ga-Ge
71Ga NMR
Ga/Ge EXAFS
Disordered Systems

ABSTRACT

$Co_3Ga_2Ge_5$ was synthesized through arc-melting stoichiometric ratios of the elements, and a Ru_3Sn_7-type structure was confirmed by X-ray diffraction. Because $Co_3Ga_2Ge_5$ contains Ga and Ge, which have very similar X-ray and neutron scattering factors, any Ga/Ge crystallographic site preference cannot be determined with diffraction alone. The purpose of this study is to highlight the importance of using multiple techniques to characterize otherwise structurally ambiguous intermetallic compounds. We utilize ^{71}Ga nuclear magnetic resonance spectroscopy and an analysis of the X-ray absorption fine structure to clarify the amount of Ga/Ge site mixing. Our combined use of X-ray diffraction and spectroscopy provides a comprehensive structural analysis of Ga site mixing across the Ge crystallographic sites, enhancing the understanding of the structure and properties of $Co_3Ga_2Ge_5$.

1. Introduction

With the growth and advancement of complex materials, bulk characterization of elements with properties has become increasingly challenging. This is particularly evident in the $R_2M_3X_5$ (R = rare earth, M = transition metal, X = main group element) family of compounds which exhibits eight different structure types and diverse physical properties such as charge density waves [1,2], quantum critical points [3,4], Kondo behavior [5,6], and giant magnetoresistance [7,8]. The junction of various physical properties [9], structural polymorphism requiring detailed synchrotron measurements [10], and potential for chemical substitution led us to study $Co_3Ga_2Ge_5$, a reported but unstudied isostructural analogue of the Ru_3Sn_7 structure [11,12]. The Ru_3Sn_7 structure type (also known as the Ir_3Ge_7 or T_3X_7 structure, with Stukturbericht classification: D_{8f}) [13] has been promoted as a tunable system with metallic, semi-metallic, and semiconducting states [14]. Notable physical properties for this structure type include hydrogen evolution catalysis [15], superconductivity [16], thermoelectric properties [17], and selective hydrogenation of acetylene [18]. $Rh_3In_{3.4}Ge_{3.6}$, a ternary analogue, has been shown to host potential Dirac nodes, revealing a topologically relevant electronic structure for this family of binary T_3X_7 compounds and its ternary analogues [19]. Like $Co_3Ga_2Ge_5$, other analogues of the Ru_3Sn_7 structure type contain elements indistinguishable by X-ray diffraction. Examples include $Nb_3Sb_2Te_5$ [17,20], $Mo_3Sb_{5.4}Te_{1.6}$ [21], Re_3GeAs_6 [22], $Co_3Al_3Si_4$ [23], $Ir_3In_3Sn_4$ [24], $Ru_3Sn_{5.25}Sb_{1.75}$ [25], and $Pt_3Tl_{5.7}Pb_{1.3}$ [26]. Atomic ordering may exist within these structures; however, the presence of crystallographic site mixing for similarly scattering elements is often overlooked. This site preference can be quantified and is influenced by factors such as bond valence and the overall stability of the crystal structure.

The problem of Ga and Ge atomic site mixing is not limited to $Co_3Ga_2Ge_5$. In $Y_4Mn_{1-x}Ga_{12-y}Ge_y$, ferromagnetism is linked to changes in Ge concentration relative to Ga [27]. The authors describe marked changes as Ge is varied from y = 1 (ferromagnetic) to y = 4 (paramagnetic). The change in magnetism is also related to Mn vacancies that

* Corresponding author.
E-mail address: Julia_Chan@baylor.edu (J.Y. Chan).

https://doi.org/10.1016/j.jallcom.2024.177828
Received 8 October 2024; Received in revised form 18 November 2024; Accepted 27 November 2024
Available online 28 November 2024

decrease as a function of Ge concentration, highlighting a link between the transition metal and Ga/Ge concentration. Another unique example is $ReGa_{0.4}Ge_{0.6}$ which displays highly localized and multicenter bonding while retaining metallic behavior [28]. To best describe the unique physical phenomena, an understanding the role of site preference in mixed Ga-Ge systems is key. However, in their investigation of the giant magnetocaloric effect present in $Gd_5Ga_xGe_{4-x}$, Gordon Miller *et al.* stated that "Ga and Ge atoms could not be unequivocally distinguished by X-ray diffraction techniques in these systems due to the one-electron difference in their electron densities [29]." The ability to use structural characterization techniques other than X-ray diffraction are vital for furthering our understanding of the structure-property relationships within these materials. In some cases, the neutron diffraction data has been analyzed to understand the degree of site mixing between similarly scattering elements. Re_3GeAs_6 [22] and $Yb_3Ga_7Ge_3$ [30] cite differences in the neutron form factors to determine site preference; however, like X-ray diffraction, there is not always a clear distinction in the neutron form factors for elements adjacent on the periodic table. This is true for Ga and Ge where the neutron coherent scattering lengths are 7.288 fm and 8.185 fm, respectively [31]. To determine the degree of atomic ordering, spectroscopic experiments to understand the Ga local environment must be employed.

In this work, we chose to implement ^{71}Ga nuclear magnetic resonance (NMR) spectroscopy and X-ray absorption spectroscopy (XAS) in combination with X-ray crystallography to determine the Ga/Ge atomic site mixing present in $Co_3Ga_2Ge_5$. NMR experiments are used with some regularity in structural studies of intermetallic compounds [32–34], and they are effective for understanding the local environment of specific elements. However, it is quite rare for NMR to be used in studying materials that contain elements that are difficult to differentiate with diffraction. $Fe_{3-x}Mn_xSi$ [35] and $Y_2(Co_{1-x}Cu_x)_{17}$ [36] highlight this underutilized application of NMR spectroscopy by observing the degree of site mixing between Fe/Mn and Co/Cu, respectively. Nuclear quadrupole resonance (NQR) spectroscopy is a similar technique to NMR that has been used to provide clarity on Ga/Ge site mixing within the structures of $ReGa_2Ge$ [37] and $ReGaGe_2$ [38]. These studies promote the efficacy of using Ga-specific probes to develop an understanding of the $Co_3Ga_2Ge_5$ structure. Additionally, element-specific Extended X-ray Absorption Fine Structure (EXAFS) analyses of the XAS are often used to determine the degree and position of site preference within problem structures [39–41]. An analysis of local structure provided by the Ga EXAFS nicely complements the description from the ^{71}Ga NMR. These techniques, along with X-ray diffraction, allow for an analysis of Ga site mixing across the two Ge crystallographic sites. In this study, we not only present the synthesis, chemical structure, and physical properties of $Co_3Ga_2Ge_5$, but also highlight powerful spectroscopic techniques that are provide chemical insight into the clarification of structures that may otherwise be difficult to probe by diffraction.

2. Methods

2.1. Synthesis

The reactions were prepared with cut pieces of the elements Co, Ga, and Ge in a 3:2:5 (Co:Ga:Ge) molar ratio. The raw elements were arc-melted into a single boule under a positive flow of Ar gas. A Zr "getter" was included in the setup to minimize oxidation of the sample. The resulting boule was flipped and re-melted three times to ensure homogeneity. Mass losses were less than 5 %. The sample was then annealed at 600 °C for 3 days. The resulting silver boule was homogeneous with a reflective surface that was resistant to oxidation. Upon inspection of the boule, large grain boundaries were observed under the microscope. An endothermic feature at 853 °C was determined by differential scanning calorimetry (DSC), indicating a congruent melting point for the material. Thermal decomposition of the material was not observed up to 1000 °C even after melting and re-solidification.

2.2. Structure determination

Pieces of the arc-melted boule were ground in an agate mortar and pestle. The powder was placed on a low-background sample holder, and powder X-ray diffraction patterns were collected on a Bruker D2 Phaser with a Cu K_α source ($\lambda = 1.54184$ Å) equipped with a LYNXEYE XE-T detector. Data were collected in the 2θ range 5 – 80 ° at room temperature and were analyzed by Rietveld refinement in TOPAS (shown in Fig. 1) [42].

Single-crystal X-ray diffraction data were obtained at room temperature from a fragment of $Co_3Ga_2Ge_5$ (approximately 0.02 ×0.03 ×0.07 mm). Data was collected using a Bruker D8 Quest Kappa single-crystal X-ray diffractometer equipped with an Incoatec IμS microfocus source (Mo K_α radiation, $\lambda = 0.71073$ Å) and a PHOTON III CPAD area detector. The raw frames were integrated with Bruker SAINT, and the intensities were corrected for absorption with a multi-scan method in SADABS 2016/2 [43]. The intrinsic phasing method in SHELXT was used to generate preliminary crystallographic models [44], which were finalized with least-squares refinements in SHELXL2019 [45]. Our best model is shown in Tables 1 and 2.

Energy-dispersive X-ray spectroscopy (EDS) was performed on a polycrystalline sample with a VERSA 3D focused ion beam scanning electron microscope to confirm the Ga:Ge ratio. The formula obtained from EDS was $Co_{2.9(3)}Ga_{1.9(5)}Ge_{5.1(4)}$, in good agreement with the nominal composition.

2.3. Solid-state nuclear magnetic resonance (NMR) spectroscopy

^{71}Ga (spin – $^3/_2$) NMR spectra were acquired using a Bruker Avance-III HD console and an 800 MHz (18.8 T) spectrometer at a Larmor frequency of 244.01 MHz. Experiments were collected using an in-house 3.2 mm triple resonance (HXY) probe under static conditions. The Quadrupolar-Carr-Purcell-Meiboom-Gill (QCPMG) pulse sequence was applied with a $\pi/2$ pulse of 1.75 μs and a recycle delay of 1 s. Due to the broad spectral band induced by the large quadrupolar couplings, a series of variable offset cumulative spectra (VOCS) were obtained using a step size of ~150 kHz. All spectra were referenced to 1.0 M $Ga(NO_3)_{3(sol)}$ at 0.0 ppm. Spectral simulation was performed using ssNake v1.4 to determine isotropic chemical shifts (δ_{iso}), quadrupolar coupling constants (Cq), and quadrupolar asymmetry parameter (η) [46].

Density functional theory (DFT) calculations were conducted using the Vienna *ab initio* simulation package (VASP), employing the projector augmented wave (PAW) method and the Perdew-Burke-Ernzerhof generalized-gradient approximation (GGA-PBE) for the exchange-correlation functional [47–49]. The latest pseudopotential files provided by VASP were utilized. For configurations involving Ga and Ge mixing, Python Materials Genomics (Pymatgen) was used to pre-screen structures with various Ga^{3+}/Ge^{4+} orderings based on the experimentally refined crystal structure of $Co_3Ga_2Ge_5$ [50]. A set of 1 × 1 × 1

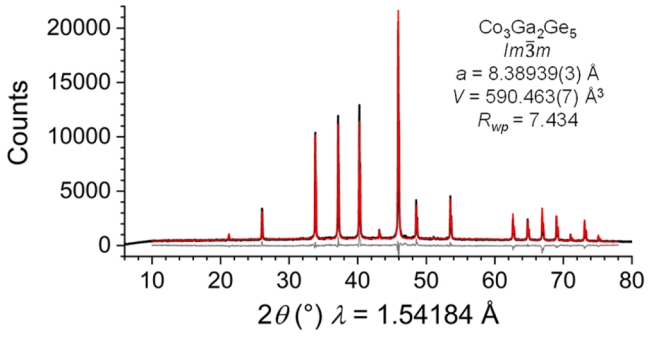

Fig. 1. Powder X-ray diffraction pattern for $Co_3Ga_2Ge_5$. Shown in black. The calculated fit from Rietveld refinement is shown in red, with the difference plot shown in grey.

Table 1
Crystallographic data, data collection, and refinement parameters (Single crystal X-ray diffraction).

Formula	$Co_3Ga_2Ge_5$
Space Group	$Im\bar{3}m$
a (Å)	8.3850(5)
V (Å^3)	589.53(11)
Z	4
Temperature (K)	298
θ (°)	3.4–30.3
μ (mm^{-1})	42.16
Measured Reflections	12937
Independent Reflections	112
R_{int}	0.068
R_σ	0.012
R_1 [$F^2 > 2\sigma(F^2)$]	0.013
wR_2 (F^2)	0.030
$\Delta\rho_{max}$, $\Delta\rho_{min}$ (e$^-$/Å^3)	0.51, −0.91
Extinction Coefficient	0.0077(4)
$R_1 = \sum\|\|F_o\| - \|F_c\|\| / \sum\|F_o\|$	
$wR_2 = \{ \sum[w(F_o^2 - F_c^2)^2] / \sum[w(F_o^2)^2] \}^{1/2}$	

Table 2
Fractional atomic coordinates and displacement parameters.

Site	Wyckoff	x	y	z	U_{eq} (Å^2)	Occ.
Co1	12*e*	0.34481 (8)	0	0	0.0078(2)	1
Ge1	12*d*	¼	0	½	0.01057(19)	5/7
Ga1	12*d*	¼	0	½	0.01057(19)	2/7
Ge2	16*f*	0.16300 (3)	0.16300(3)	0.16300 (3)	0.00878(18)	5/7
Ga2	16*f*	0.16300 (3)	0.16300(3)	0.16300 (3)	0.00878(18)	2/7

supercells were generated, and electrostatic energy calculations for these supercells were performed using Ewald summation techniques [51]. Geometry optimization was carried out with DFT calculations, and the isotropic chemical shifts of the relaxed structures were computed using perturbation theory (linear response) [52,53]. The nuclear quadrupole moment for each nucleus was specified to determine the quadrupolar constant [54,55].

2.4. X-ray absorption spectroscopy (XAS)

The Co, Ga, and Ge K-edges for $Co_3Ga_2Ge_5$ were measured at 6-BM at the National Synchrotron Light Source II (NSLS-II). Scans were collected at room temperature in transmission mode using a flat mirror designed for rejecting harmonic frequencies. Metal foils were simultaneously measured as references. The sample was ground together with boron nitride in a mixture to target an edge step value of 1. The powder was then loaded into a sample wheel, where the front and back of the sample was covered with Kapton tape. Three scans were taken at each edge. Scans 2 and 3 were aligned with scan 1. All manipulations of the data and fitted models were done in the Demeter XAS software package (ATHENA and ARTEMIS) [56]. After alignment, the 3 scans were normalized and averaged together in ATHENA. Analysis of the EXAFS region was conducted with the Artemis software. FEFF calculations for each main group crystallographic site (12*d* and 16*f*) were generated using IFEFFIT through the ARTEMIS interface. Fits to the Ga EXAFS region were analyzed first for the 12*d* and 16*f* Ga/Ge sites separately, then both crystallographic sites were considered together to achieve a better fit to the data.

2.5. Physical properties

A 17 mg polished piece of the arc-melted boule was prepared for the physical property measurements. Temperature-dependent magnetization data were collected using a Quantum Design MPMS system. The sample was zero-field-cooled (ZFC), then measured on warming 1.8 – 300 K in an external magnetic field of 0.5 T. The field-dependent magnetization data were collected at 1.8 K in a range −7 – 7 T. The electrical resistance was measured on the same sample in a Quantum Design PPMS system. A standard 4-probe method was employed, where each probe consisted of 0.002 in. diameter Pt wire attached with silver paste. A current of 700 μA was applied, and resistance was measured on cooling in a temperature range of 300 – 2 K.

3. Results and discussion

3.1. Average structure of $Co_3Ga_2Ge_5$

The detailed structural investigation of compounds adopting the Ru_3Sn_7 structure type is critical to understanding the bulk physical properties expressed by the various binary and ternary analogues. The structural motifs of Ru_3Sn_7 and its analogues have been described in a few ways. Viewing this structure as lattice complexes (Dirichlet domains) or a collection of concentric clusters allow for direct structural comparisons to the γ-brass and Sb_2Tl_7 structure types [57,58]. However, the most prevalent description presents the Ru_3Sn_7 system as interpenetrating frameworks of face-sharing, square antiprisms [59,60]. When considering this view, a distinction is made between the three crystallographic sites (Ru1: 12*e*, Sn1: 12*d*, and Sn2: 16*f*) through the isolated framework. This allows an easier view of which atomic site(s) may be substituted as a third element is incorporated into the structure. The antiprisms of Ru_3Sn_7 form three dimensional barrels around an empty Sn_8 cube, where Ru—Ru dimers are contained within these barrels (Fig. 2).

Investigations into the stability of the T_3X_7 compounds have shown a dependency on Valence Electron Counting (VEC), highlighting the flexibility of its bonding [14]. Further work has extended the VEC approach into a useful electron counting equation normalized to the transition metal: 18-n+m, where n and m are the degree of T-T and X-X bonding interactions, respectively [61,62]. Upon the introduction of a third element to the Ru_3Sn_7 structure type (such as another main-group element), the total VEC (or n- and m-terms) can be optimized to form ternary compounds from otherwise unstable binary combinations. A range of VECs between 51 and 55 are typically observed for binary and ternary analogues of this structure type. Hypothetically, the binary Co_3Ge_7 would have a VEC of 55 (18.33/Co atom). This may be near the edge of stability for the Ru_3Sn_7 structure type and should be isoelectronic to Ir_3Ge_7. In contrast to Ir_3Ge_7, Co_3Ge_7 has not been observed

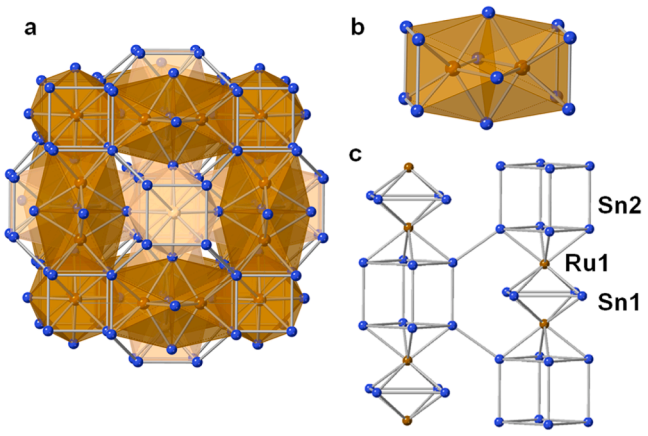

Fig. 2. Framework representation of the Ru_3Sn_7 structure: a) Interpenetrating square antiprisms, b) Ru—Ru dimer within square antiprism barrel, and c) isolated framework with atomic sites.

experimentally and may exist only as a metastable structure in the Co-Ge phase space. By replacing two stoichiometric equivalents of Ge with Ga in $Co_3Ga_2Ge_5$, the VEC is lowered to 53 (17.67/Co atom), falling further into the midpoint for the range of stability exhibited by this structure type. It should be noted that in the initial report for $Co_3Ga_2Ge_5$, the authors described a small range of composition for Ge: 44–52 at% [11]. Based on the minimal mass losses in preparing the samples and composition from EDS, we do not observe large changes from the nominal composition; however, the VEC could deviate from integer values with these small changes in stoichiometry. Regardless of the amount, an introduction of a third element provokes the question: How does the incorporated element populate the structure?

The challenge for understanding the structure of $Co_3Ga_2Ge_5$ is that Ga and Ge have similar scattering factors and are, therefore, virtually indistinguishable with typical diffraction experiments. The indistinguishability problem is also convoluted by the possible structural models that can be used to describe this system. There are three practical structural models to consider (Fig. 3):

The first cubic $Im\bar{3}m$ model (a) contains no Ga/Ge site ordering, and the main group atoms fill the structure in a solid solution. The Ga and Ge atoms are mixed in a 2:5 ratio on all grey 12*d* and 16*f* sites. The next cubic $Im\bar{3}m$ model (b) contains complete Ge site ordering on one main group site (Ge occupies the dark blue 12*d* site), while the other site is mixed (Ga and Ge occupy the 16*f* site in a 1:1 ratio). The third, cubic $I\bar{4}3m$ model (c) is lower in symmetry and has complete Ga and Ge site preference. Due to the reduction in symmetry, the 16*f* site from the $Im\bar{3}m$ models becomes two unique 8*c* sites in the $I\bar{4}3m$ model. One 8*c* site (dark blue) is only occupied by Ge, and the other 8*c* site (cyan) is only occupied by Ga. The dark blue *12d* site is only occupied by Ge.

Both single crystal and powder X-ray diffraction data were collected from the samples of $Co_3Ga_2Ge_5$. For both datasets, a cubic, *I*-centered lattice was indexed with an unit cell consistent with the Ru_3Sn_7 structure type. The distances between Co and the main group elements for $Co_3Ga_2Ge_5$ are (Co-Ga/Ge1) x 4: 2.4674(4) Å and (Co-Ga/Ge2) x 4: 2.4617(5) Å. These distances are within the range of distances expected for both intermetallic Co-Ga and Co-Ge bonds, so no site preference could be distinguished based on the atomic distances. Therefore, both Ga and Ge were allowed to mix on both atomic positions. Occupancies of Ga and Ge on these two sites were constrained based on the nominal composition and the values obtained from EDS, representing an even distribution of Ga:Ge across both atomic sites in a 2:5 ratio (Table 2).

Based on X-ray diffraction techniques alone, the three presented models for $Co_3Ga_2Ge_5$ are indistinguishable from one another. This is in contrast to $Rh_3In_{3.4}Ge_{3.6}$, where In and Ge are distinguishable with X-ray crystallography and a strong site preference for the In and Ge atoms is observed on the 12*d* and 16*f* atomic sites, respectively [19]. The authors say that better crystallographic refinements are achieved with In/Ge site mixing on both main group sites (12*d*: 91 % In, 9 % Ge and 16*f*: 16 % In, 84 % Ge). This allows for the crystallographic refinement of the non-integer formula $Rh_3In_{3.4}Ge_{3.6}$ and is supported by elemental analysis. Rhodium and cobalt are isoelectronic as well as In and Ga, making this a good system to compare the VEC to $Co_3Ga_2Ge_5$. $Rh_3In_{3.4}Ge_{3.6}$ has a VEC of 51.6 (17.2/Rh atom). The authors highlight a contracted Rh-Rh distance (3.008(2) Å), which would correspond to a stronger M-M interaction and a higher *n*-term, lowering the VEC and supporting the 18-*n*+*m* rule. If the small amount of site mixing is ignored, the distances between the Rh and main group elements can be distinguished: (Rh-In1) x4: 2.7065(4) Å and (Rh-Ge2) x4: 2.5770(6) Å. In comparison to $Co_3Ga_2Ge_5$, the Co-Ga/Ge1 and Co-Ga/Ge2 distances are nearly identical. This difference supports a structure for $Co_3Ga_2Ge_5$ with no Ga ordering across both main group atomic sites. However, the disparity in the Rh-In and Rh-Ge bonds could be explained by the differences in In and Ge size. Ga and Ge do not have a large size difference; therefore, other techniques must be used to confirm Ga/Ge site mixing. To gain a complete understanding of the structure of $Co_3Ga_2Ge_5$, one must also consider the local structure of the Ga and Ge atoms.

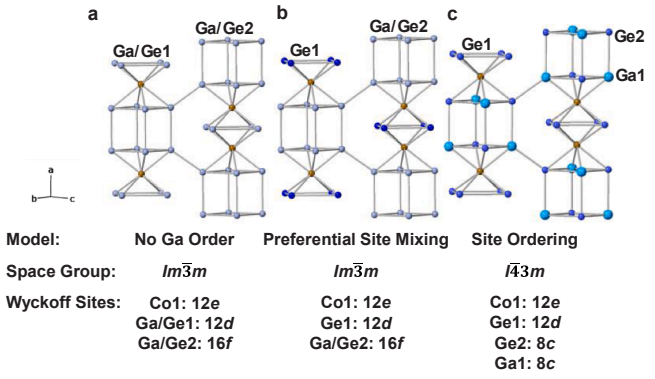

Fig. 3. Isolated fragments of $Co_3Ga_2Ge_5$ showing the possible crystallographic models for Ga substitution. Co (brown), Ga (cyan), Ge (dark blue), and Mixed Ga/Ge Sites (grey).

3.2. *Local structure of $Co_3Ga_2Ge_5$*

^{71}Ga NMR spectroscopy and an analysis of the Ga extended X-ray absorption fine structure (EXAFS) were utilized to determine the effect of Ga substitution on the 12*d* and 16*f* Ge crystallographic sites in $Co_3Ga_2Ge_5$. It should be noted that NMR and EXAFS are not the only spectroscopic techniques that can used to describe Ga or Ge local environments. In a study of site preference for $Nb_3Sb_2Te_3$, Sb Mössbauer was used to distinguish Sb from Te [63]. Ga Mössbauer experiments were not probed for $Co_3Ga_2Ge_5$, because Ga is not a suitable nucleus for Mössbauer experiments. Analyses of the ^{73}Ge NMR or Ge Mössbauer spectroscopies were abandoned, because Ge will occupy both the 12*d* and 16*f* crystallographic sites. Therefore, any information about the site preference of Ga substitution on Ge crystallographic sites must be determined through an investigation into the Ga local environment. An analysis of the Ge EXAFS is detailed in the supplemental information and is used as a comparison to the Ga EXAFS.

For nuclei with a spin greater than ½, such as ^{71}Ga (S=3/2), structural deviations from perfect cubic symmetry can yield non-vanishing quadrupolar coupling interactions, resulting in broad NMR spectra. Therefore, the quadrupole coupling constant (Cq) provides a sensitive measure of the local environment around gallium (Ga) [64]. Hence, ^{71}Ga NMR spectroscopy is an invaluable tool for probing nuanced changes in the local crystallographic environment of Ga atoms. The ^{71}Ga NMR spectrum of $Co_3Ga_2Ge_5$ (lower right-hand side of Fig. 4) is extremely broad under static conditions with a bandwidth of nearly ~ 1 MHz. Spectral deconvolution reveals two distinct Ga sites with experimental isotropic shifts resonating at 1630 ppm and 1580 ppm for sites 1 and 2, respectively. The experimental Cq values of Ga1 and Ga2 sites are 38.85 and 30.85 MHz. To confirm the presence of two distinct sites, the three proposed structural models were utilized for DFT NMR calculation. The DFT NMR calculations using VASP and the PAW approach reveal a decrease in Cq values from no Ga/Ge ordering to complete Ga/Ge site preference (shown on the left-hand side of Fig. 4), indicating progressive structural order. Notably, the calculated Cq values of the complete Ga/Ge site mixing (12*d*: 30.42 MHz and 16*f*: 30.28 MHz) show relatively good agreement with the experimentally observed Cq values, thereby confirming the presence of two distinct Ga sites and no Ga/Ge site ordering as depicted in Figs. 3a and 4.

Due to its element specificity, we also collected EXAFS data at the Co, Ga, and Ge K-edges. We tested multiple fit models against the data to probe the presence and extent of Ga/Ge site mixing. We note that EXAFS fitting contains its own set of assumptions and caveats, and changes in the number of parameters may not necessarily improve a fitting model [65]; however, we present a model that is consistent with the ^{71}Ga NMR, further supporting site mixing across both the 12*d* and 16*f* atomic sites.

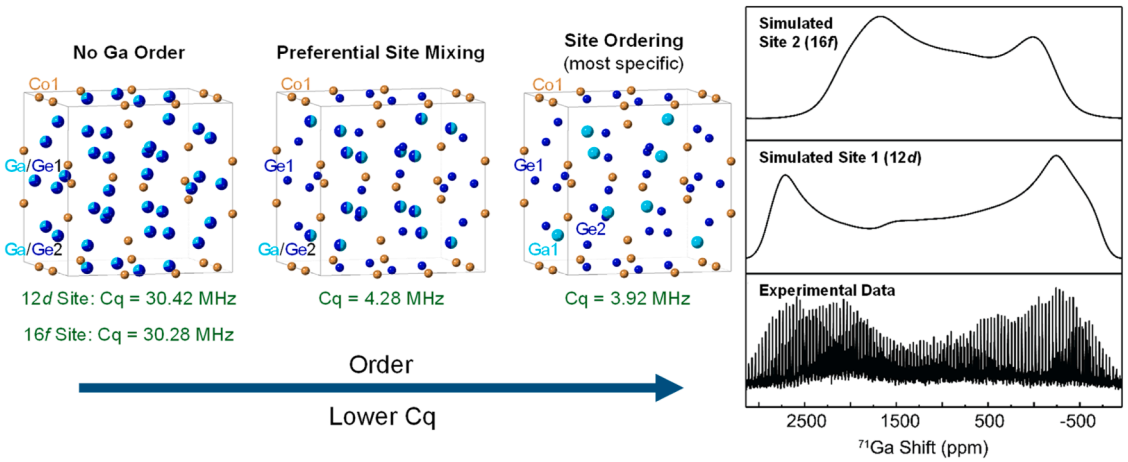

Fig. 4. Unit cell representations of the models outlined in Fig. 2 with the ^{71}Ga NMR spectrum. Calculated spectra for the No Ga Order Model Site 1 (12*d*, Cq = 30.42 MHz) and Site 2 (16*f*, Cq = 30.28 MHz) are also shown.

More information on the fits to the Co, Ga, and Ge EXAFS and their statistics are included in the supplemental information as well as other EXAFS plots used in the analysis. By selecting scattering paths from both atomic positions for the fit, χ^2 and the R-factor are reduced. The improvement is shown in Fig. 5, where the fit with both sites (red) more closely follows the radial distribution of the data (black) across the entire fitting range. The 12*d* atomic site (blue) more clearly fits the data in the 3.0 – 4.0 Å range; however, the 16*f* atomic site (pink) is necessary for fitting the radial distances above 4.5 Å.

While neither of these methods on their own contribute to a complete picture of the local structure, together the NMR and EXAFS both point to a consistent model—there is site mixing between the Ga and Ge atoms. The ^{71}Ga NMR experiments clearly show two signals with area integrals in a 55:45 ratio. This is very close to the ratio of the multiplicities for the 16*f* and 12*d* atomic sites: 4:3 (60:45 for comparison), representing an even distribution of Ga across both atomic sites. Resolving the nearest neighbors of the Ga coordination sphere is impossible from the NMR spectrum alone. The fit to the EXAFS region of the XAS, while subject to over-fitting and small changes in the variables, allows for another evaluation of the local symmetry, confirming the site-mixing model. This is supported by an improvement of the fit statistics when both crystallographic sites are considered. Furthermore, when both spectroscopy techniques are considered together, the picture becomes clear. Gallium is occupying both the 12*d* and 16*f* crystallographic sites within the structure. Previous reports of ternary Ru_3Sn_7-type compounds indicate at least some site preference for the substituted atom [17,19,21]. Our findings differ, pointing towards very little or no site preference for gallium on the germanium crystallographic sites.

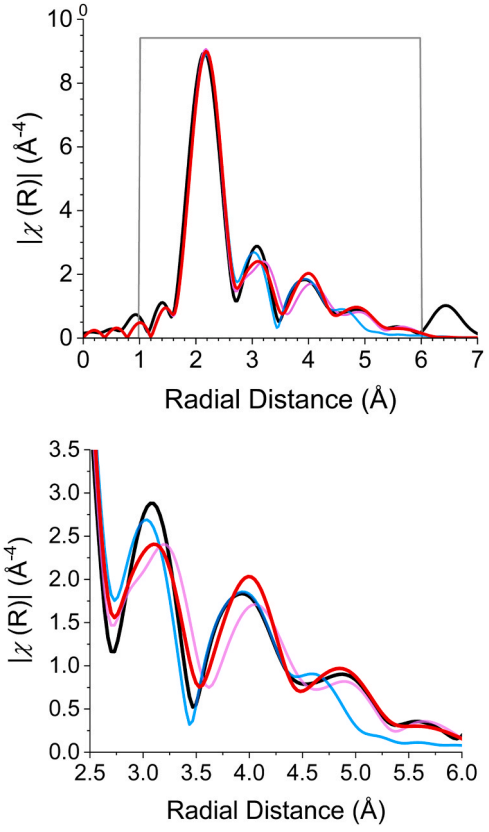

Fig. 5. Top: The Ga EXAFS region (black) with fits using the 12*d* antiprism site paths (pink), the 16*f* cube site paths (blue), and paths from both crystallographic sites (red). Bottom: Zoomed to show the difference between the fits.

3.3. *Physical properties of $Co_3Ga_2Ge_5$*

Fig. 6 shows the temperature-dependent resistivity of $Co_3Ga_2Ge_5$. The increase of the resistivity with increasing temperature is consistent with a typical metallic behavior. The temperature-dependent magnetic susceptibility χ(T) and the field-dependent magnetization *M*(H) of $Co_3Ga_2Ge_5$ are included in the Supporting Information. Our measurements agree with the behavior of a temperature independent paramagnet.

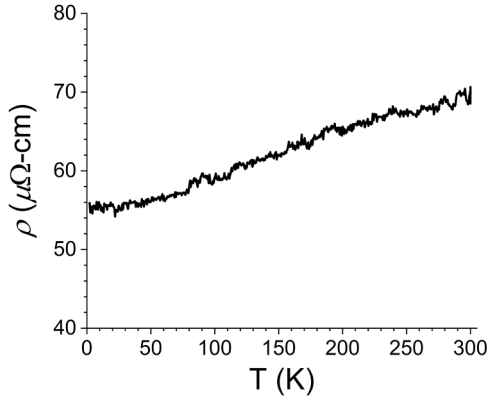

Fig. 6. Temperature-dependent resistivity of $Co_3Ga_2Ge_5$ from 2 K to 300 K.

4. Conclusion

The techniques used in this paper highlight a need in intermetallic research for utilizing multiple methods of characterization. Diffraction techniques are not suitable for distinguishing between elements of similar size and atomic number like Ga and Ge; however, incorporating elements with similar X-ray and neutron scattering factors is common for studies aimed at tuning the band structure of materials. Using a spectroscopic approach is important to remedying any structural confusion. Since the Ru_3Sn_7 structure has potential for hosting topological properties, it is vital to develop an understanding of how a third element affects the binary structure. A reduction in centrosymmetry would allow for the chemical tuning of the band structure, potentially creating Weyl nodes from Dirac nodes. For $Co_3Ga_2Ge_5$, this is not the case. The study presented herein shows no site preference for Ga across the two Ge sites, implying no change in the average and local structure symmetries. Analysis of both the ^{71}Ga NMR and Ga EXAFS confirm a model containing two crystallographic sites for the Ga atoms. While a model with Ga site preference is not justified for $Co_3Ga_2Ge_5$, further substitution studies with elements that can create structural distortions could have a large impact on the properties of the material or isostructural analogues. This would not only generate interest in finding other binary structures that have the potential to be altered with a third element, but also highlight the significance of understanding how topologically relevant, Ru_3Sn_7-type compounds can be fine-tuned on a structural level. We hope that this investigation of $Co_3Ga_2Ge_5$ inspires other studies to utilize multiple characterization methods for compounds that may seem ambiguous from the diffraction data alone.

CRediT authorship contribution statement

Julia Y. Chan: Writing – review & editing, Supervision, Funding acquisition, Data curation, Conceptualization. **W. Kice Brown:** Writing – review & editing, Writing – original draft, Visualization, Validation, Methodology, Investigation, Formal analysis, Data curation, Conceptualization. **Ifeoluwa P. Oyekunle:** Writing – review & editing, Writing – original draft, Investigation, Formal analysis. **Erica Truong:** Writing – review & editing, Writing – original draft, Investigation, Formal analysis. **Yudan Chen:** Writing – review & editing, Investigation, Formal analysis. **Kaya Wei:** Writing – review & editing, Supervision, Investigation, Funding acquisition, Formal analysis, Data curation, Conceptualization. **Gregory T. McCandless:** Writing – review & editing, Formal analysis, Data curation. **Yan-Yan Hu:** Writing – review & editing, Supervision, Funding acquisition, Formal analysis, Data curation. **Bright Ogbolu:** Writing – review & editing, Investigation, Formal analysis. **Benny Schundelmier:** Writing – review & editing, Writing – original draft, Investigation, Formal analysis, Data curation, Conceptualization. **Shaun O'Donnell:** Writing – review & editing, Validation, Investigation, Data curation. **Rebecca W. Smaha:** Writing – review & editing, Supervision, Funding acquisition, Formal analysis, Data curation.

Declaration of Competing Interest

The authors declare that they have no known competing financial interests or personal relationships that could have appeared to influence the work reported in this paper.

Acknowledgements

J.Y.C. gratefully acknowledges the support of both the Welch Foundation, AA-2056-20220101 and the U.S. Department of Energy, DE-SC0022854. A portion of this work was performed at the National High Magnetic Field Laboratory (NHMFL), which is supported by National Science Foundation Cooperative Agreement No. DMR-1644779, DMR-2128556, and the State of Florida. This work was also authored in part by the National Renewable Energy Laboratory, operated by Alliance for Sustainable Energy, LLC, for the DOE under Contract No. DE-AC36-08GO28308. Funding for XAS data collection was provided by the U.S. Department of Energy, Office of Science, Basic Energy Sciences, Division of Materials Science, through the Office of Science Funding Opportunity Announcement (FOA) Number DE-FOA-0002676: Chemical and Materials Sciences to Advance Clean-Energy Technologies and Transform Manufacturing. E.T., I.P.O., B.O., Y.C., and Y.-Y.H. acknowledge the support from the National Science Foundation under grant no. DMR-1847038. B.S. and K.W. acknowledge the support of the NHMFL User Collaboration Grant Program (UCGP). The authors also thank Dr. Bruce Ravel for assistance with XAS beamtime. The views expressed in the article do not necessarily represent the views of the DOE or the U.S. Government.

Accession codes

CCDC 2373028 contains the supplementary crystallographic data for this paper. These data can be obtained free of charge via www.ccdc.cam.ac.uk/data_request/cif, by emailing data_request@ccdc.cam.ac.uk, or by contacting the Cambridge Crystallographic Data Center, 12 Union Road, Cambridge CB2 1EZ, UK; fax: +44 1223 336033.

Appendix A. Supporting information

Supplementary data associated with this article can be found in the online version at doi: 10.1016/j.jallcom.2024.177828.

Data Availability

Data will be made available on request.

References

[1] M.H. Lee, C.H. Chen, M.W. Chu, C.S. Lue, Y.K. Kuo, Electronically phase-separated charge-density waves in $Lu_2Ir_3Si_5$, Phys. Rev. B 83 (2011) 155121.
[2] D.E. Bugaris, C.D. Malliakas, F. Han, N.P. Calta, M. Sturza, M.J. Krogstad, R. Osborn, S. Rosenkranz, J.P.C. Ruff, G. Trimarchi, et al., Charge density wave in the new polymorphs of $RE_2Ru_3Ge_5$ (RE = Pr, Sm, Dy), J. Am. Chem. Soc. 139 (2017) 4130–4143.
[3] R. Khan, Q. Mao, H. Wang, J. Yang, J. Du, B. Xu, Y. Zhou, Y. Zhang, B. Chen, M. Fang, Quantum Critical Behavior in an Antiferromagnetic Heavy-fermion Kondo Lattice System $(Ce_{1-x}La_x)_2Ir_3Ge_5$, Chin. Phys. B 26 (2017) 017401.
[4] R. Khan, K. Althubeiti, M. Algethami, N. Rahman, M. Sohail, Q. Mao, Q. Zaman, A. Ullah, N. Ilyas, A. Mohammad Afzal, et al., Observation of quantum criticality in antiferromagnetic based $(Ce_{1-x}Y_x)_2Ir_3Ge_5$ Kondo-lattice system, J. Magn. Magn. Mater. 556 (2022) 169361.
[5] Z. Hossain, H. Ohmoto, K. Umeo, F. Iga, T. Suzuki, T. Takabatake, N. Takamoto, K. Kindo, Antiferromagnetic Kondo-lattice systems $Ce_2Rh_3Ge_5$ and $Ce_2Ir_3Ge_5$ with moderate heavy-fermion behavior, Phys. Rev. B 60 (1999) 10383–10387.
[6] M.B. Gamża, R. Gumeniuk, U. Burkhardt, W. Schnelle, H. Rosner, A. Leithe-Jasper, A. Ślebarski, Coexistence of magnetic order and valence fluctuations in the Kondo lattice system $Ce_2Rh_3Sn_5$, Phys. Rev. B 95 (2017) 165142.
[7] C. Mazumdar, A.K. Nigam, R. Nagarajan, C. Godart, L.C. Gupta, B.D. Padalia, G. Chandra, R. Vijayaraghavan, Positive giant magnetoresistance in antiferromagnetic $RE_2Ni_3Si_5$ (RE=Tb, Sm, Nd), Appl. Phys. Lett. 68 (1996) 3647–3649.
[8] R. Nirmala, S.K. Malik, A.V. Morozkin, Y. Yamamoto, H. Hori, Large magnetoresistance in intermetallic compounds $R_2Mn_3Si_5$ (R = Tb, Dy and Ho), Europhys. Lett. 76 (2006) 471.
[9] W.K. Brown, M.A. Plata, M.E. Raines, J.Y. Chan, Chapter 330 - Structural and Physical Properties of $R_2M_3X_5$ Compounds, in: J.-C.G. Bunzli, S.M. Kauzlarich (Eds.), EdsIn Handbook on the Physics and Chemistry of Rare Earths, 64, Elsevier, 2023, pp. 1–92.
[10] T.M. Kyrk, E.R. Kennedy, J. Galeano-Cabral, G.T. McCandless, M.C. Scott, R. E. Baumbach, J.Y. Chan, Much More to Explore with an Oxidation State of Nearly Four: Pr Valence Instability in Intermetallic *m*-$Pr_2Co_3Ge_5$, Sci. Adv. 10 (2024) eadl2818.
[11] P.K. Panday, K. Schubert, Strukturuntersuchungen in Einigen Mischungen T-B^3-B^4 (T=Mn, Fe, Co, Ir, Ni, Pd; B3= Al, Ga, Tl; B4=Si, Ge), J. Less-Common Met. 18 (1969) 175–202.
[12] K.P. Gupta, The Co-Ga-Ge (Cobalt-Gallium-Germanium) system, J. Ph. Equilib. Diff. 27 (2006) 513–516.
[13] O. Nial, X-ray studies on binary alloys of tin with transition metals, Sven. Kem. Tidskr. 59 (1947) 172–177.

[14] U. Häussermann, M. Elding-Pontén, C. Svensson, S. Lidin, Compounds with the Ir_3Ge_7 structure type: interpenetrating frameworks with flexible bonding properties, Chem. Eur. J. 4 (1998) 1007–1015.
[15] Z. Wang, Z. Lin, Y. Wang, S. Shen, Q. Zhang, J. Wang, W. Zhong, Nontrivial topological surface states in Ru_3Sn_7 toward wide pH-range hydrogen evolution reaction, Adv. Mater. 35 (2023) 2302007.
[16] Z. Bukowski, D. Badurski, J. Stępień-Damm, R. Troć, Single crystal growth and superconductivity of Mo_3Sb_7, Solid State Commun. 123 (2002) 283–286.
[17] N. Soheilnia, J. Giraldi, A. Assoud, H. Zhang, T.M. Tritt, H. Kleinke, Thermoelectric properties of $Nb_3Sb_2Te_5$, J. Alloy. Compd. 448 (2008) 148–152.
[18] J. Osswald, R. Giedigkeit, R.E. Jentoft, M. Armbrüster, F. Girgsdies, K. Kovnir, T. Ressler, Y. Grin, R. Schlögl, Palladium–gallium intermetallic compounds for the selective hydrogenation of acetylene: Part I: preparation and structural investigation under reaction conditions, J. Catal. 258 (2008) 210–218.
[19] A.F. Savvidou, J.K. Clark, H. Wang, K. Wei, E.S. Choi, S. Mozaffari, X. Qian, M. Shatruk, L. Balicas, Complex dirac-like electronic structure in atomic site-ordered $Rh_3In_{3.4}Ge_{3.6}$, Chem. Mater. 33 (2021) 1218–1227.
[20] P. Jensen, A. Kjekshus, The crystal structure of $Nb_3Sb_2Te_5$, J. Less-Common Met. 13 (1967) 357–359.
[21] C. Candolfi, B. Lenoir, A. Dauscher, J. Tobola, S.J. Clarke, R.I. Smith, Neutron diffraction and Ab initio studies of Te Site preference in $Mo_3Sb_{7-x}Te_x$, Chem. Mater. 20 (2008) 6556–6561.
[22] N. Soheilnia, H. Xu, H. Zhang, T.M. Tritt, I. Swainson, H. Kleinke, Thermoelectric properties of $Re_3Ge_{0.6}As_{6.4}$ and Re_3GeAs_6 in comparison to $Mo_3Sb_{5.4}Te_{1.6}$, Chem. Mater. 19 (2007) 4063–4068.
[23] K.O. Burger, A. Wittmann, H. Nowotny, Die Kristallstruktur von $Co_3Al_3Si_4$ und Co_2AlSi_2 und der Aufbau einiger Monosilicidsysteme von Übergangsmetallen, Mon. Chem. Verw. Teil. And. Wiss. 93 (1962) 9–14.
[24] F. Hulliger, New T_3B_7 compounds, Nature 209 (1966) 500–501.
[25] C. Lv, X. Cheng, J. Sui, K. Jia, X. Dong, M. Ding, B. Pan, Superconductivity of a new Ru-based alloy $Ru_3Sb_{1.75}Sn_{5.25}$, Phys. B: Condens. 677 (2024) 415733.
[26] K. Schubert, S. Bhan, T.K. Biswas, K. Frank, P.K. Panday, Einige Strukturdaten Metallischer Phasen, Sci. Nat. 55 (1968) 542–543.
[27] M.C. Francisco, C.D. Malliakas, P.M.B. Piccoli, M.J. Gutmann, A.J. Schultz, M. G. Kanatzidis, Development and loss of ferromagnetism controlled by the interplay of Ge concentration and Mn vacancies in structurally modulated $Y_4Mn_{1-x}Ga_{12-y}Ge_y$, J. Am. Chem. Soc. 132 (2010) 8998–9006.
[28] M.S. Likhanov, V.Y. Verchenko, A.N. Kuznetsov, A.V. Shevelkov, $ReGa_{0.4}Ge_{0.6}$: intermetallic compound with pronounced covalency in the bonding pattern, Inorg. Chem. 58 (2019) 2822–2832.
[29] S. Misra, Y. Mozharivskyj, A.O. Tsokol, D.L. Schlagel, T.A. Lograsso, G.J. Miller, Structural, Magnetic, and Thermal Characteristics of the Phase Transitions in $Gd_5Ga_xGe_{4-x}$ Magnetocaloric Materials. J. Solid State Chem. 182 (2009) 3031–3040.
[30] S.C. Peter, C.D. Malliakas, H. Nakotte, K. Kothapilli, S. Rayaprol, A.J. Schultz, M. G. Kanatzidis, The Polygallides: $Yb_3Ga_7Ge_3$ and $YbGa_4Ge_2$, J. Solid State Chem. 187 (2012) 200–207.
[31] V.F. Sears, Neutron Scattering Lengths and Cross Sections, Neutron N. 3 (1992) 26–37.
[32] E. Dormann, Chapter 94 NMR in Intermetallic Compounds, in: In *Handbook on the Physics and Chemistry of Rare Earths*, 14, Elsevier, 1991, pp. 63–161.
[33] C. Benndorf, H. Eckert, O. Janka, Structural characterization of intermetallic compounds by ^{27}Al solid state NMR spectroscopy, Acc. Chem. Res. 50 (2017) 1459–1467.
[34] J.M. Gerdes, L. Schumacher, M.R. Hansen, R. Pöttgen, A solid-state ^{171}Yb NMR-spectroscopic characterization of selected divalent ytterbium intermetallics, Z. Naturforsch. B Chem. Sci. 79 (2024) 13–19.
[35] V. Niculescu, K. Raj, T.J. Burch, J.I. Budnick, Correlation of the internal fields, magnetic moments, and site preferences in $Fe_{3-x}Mn_xSi$ alloys, Phys. Rev. B 13 (1976) 3167–3174.
[36] K. Inomata, Individual Co site contributions to the magnetic anisotropy and NMR investigation of $Y_2(Co_{1-x}M_x)_{17}$ (M = Cu, Al), Phys. Rev. B 23 (1981) 2076–2081.
[37] M.S. Likhanov, V.Y. Verchenko, A.A. Gippius, S.V. Zhurenko, A.V. Tkachev, Z. Wei, E.V. Dikarev, A.N. Kuznetsov, A.V. Shevelkov, Electron-precise semiconducting $ReGa_2Ge$: extending the $IrIn_3$ structure type to group 7 of the periodic table, Inorg. Chem. 59 (2020) 12748–12757.
[38] M.S. Likhanov, R.A. Khalaniya, V.Y. Verchenko, A.A. Gippius, S.V. Zhurenko, A. V. Tkachev, D.I. Fazlizhanova, A.N. Kuznetsov, A.V. Shevelkov, $ReGaGe_2$: an intermetallic compound with semiconducting properties and localized bonding, Chem. Commun. 55 (2019) 5821–5824.
[39] A. Umicevic, H.-E. Mahnke, J. Belosevic-Cavor, B. Cekic, G. Schumacher, I. Madjarevic, V. Koteski, Site preference and lattice relaxation around 4*d* and 5*d* refractory elements in Ni_3Al, J. Synchrotron Radiat. 23 (2016) 286–292.
[40] X. Chi, Y. Li, X.-h Han, X.-l Duan, J.-b Sun, C.-x Cui, A New $Sm(Co,Fe,Cu)_4B$/$Sm_2(Co,Fe,Cu)_7$ Cell Structure with the Coercivity of up to 5.01 T. J. Magn. Magn. Mater. 458 (2018) 66–74.
[41] T. Bartoli, K. Zehani, J. Moscovici, A. Michalowicz, L. Bessais, EXAFS unraveling of the Fe substitution sites in high anisotropic nanocrystalline $Pr(Co,Fe)_3$, J. Magn. Magn. Mater. 473 (2019) 253–261.
[42] A. Coelho, TOPAS and TOPAS-academic: an optimization program integrating computer algebra and crystallographic objects written in C++, J. Appl. Crystallogr. 51 (2018) 210–218.
[43] L. Krause, R. Herbst-Irmer, G.M. Sheldrick, D. Stalke, Comparison of silver and molybdenum microfocus X-ray sources for single-crystal structure determination, J. Appl. Crystallogr. 48 (2015) 3–10.
[44] G. Sheldrick, SHELXT - Integrated space-group and crystal-structure determination, Acta Crystallogr. A. 71 (2015) 3–8.
[45] G. Sheldrick, Crystal structure refinement with SHELXL, Acta Crystallogr. C. 71 (2015) 3–8.
[46] S.G.J. van Meerten, W.M.J. Franssen, A.P.M. Kentgens, ssNake: a cross-platform open-source NMR data processing and fitting application, J. Magn. Reson. 301 (2019) 56–66.
[47] P.E. Blöchl, Projector augmented-wave method, Phys. Rev. B 50 (1994) 17953–17979.
[48] G. Kresse, J. Furthmüller, Efficient iterative schemes for *ab initio* total-energy calculations using a plane-wave basis set, Phys. Rev. B 54 (1996) 11169–11186.
[49] J.P. Perdew, K. Burke, M. Ernzerhof, Generalized Gradient Approximation Made Simple, Phys. Rev. Lett. 77 (1996) 3865–3868.
[50] S.P. Ong, W.D. Richards, A. Jain, G. Hautier, M. Kocher, S. Cholia, D. Gunter, V. L. Chevrier, K.A. Persson, G. Ceder, Python materials genomics (pymatgen): a robust, open-source python library for materials analysis, Comput. Mater. Sci. 68 (2013) 314–319.
[51] A.Y. Toukmaji, J.A. Board, Ewald summation techniques in perspective: a survey, Comput. Phys. Commun. 95 (1996) 73–92.
[52] C.J. Pickard, F. Mauri, All-electron magnetic response with pseudopotentials: NMR chemical shifts, Phys. Rev. B 63 (2001) 245101.
[53] J.R. Yates, C.J. Pickard, F. Mauri, Calculation of NMR chemical shifts for extended systems using ultrasoft pseudopotentials, Phys. Rev. B 76 (2007) 024401.
[54] P. Pyykkö, Year-2008 Nuclear Quadrupole Moments, Mol. Phys. 106 (2008) 1965–1974.
[55] P. Pyykkö, Year-2017 Nuclear Quadrupole Moments, Mol. Phys. 116 (2018) 1328–1338.
[56] B. Ravel, M. Newville, Athena, Artemis, Hephaestus: Data analysis for X-ray absorption spectroscopy using IFEFFIT, J. Synchrotron Radiat. 12 (2005) 537–541.
[57] R. Stokhuyzen, C. Chieh, W.B. Pearson, Crystal Structure of Sb_2Tl_7, Can. J. Chem. 55 (1977) 1120–1122.
[58] E. Hellner, E. Koch, A comparison of the crystal structures of Sb_2Tl_7, Cu_5Zn_8 (γ-Brass), and Ir_3Ge_7, Can. J. Chem. 58 (1980) 708–713.
[59] B.C. Chakoumakos, D. Mandrus, Ru_3Sn_7 with the Ir_3Ge_7 structure-type, J. Alloy. Compd. 281 (1998) 157–159.
[60] L. Eriksson, J. Lanner, Ru_3Sn_7, a Re-investigation, Acta Crystallogr. E 57 (2001) i85–i86.
[61] V.J. Yannello, B.J. Kilduff, D.C. Fredrickson, Isolobal analogies in intermetallics: the reversed approximation MO approach and applications to $CrGa_4$- and Ir_3Ge_7-type phases, Inorg. Chem. 53 (2014) 2730–2741.
[62] V.J. Yannello, D.C. Fredrickson, Generality of the 18-n rule: intermetallic structural chemistry explained through isolobal analogies to transition metal complexes, Inorg. Chem. 54 (2015) 11385–11398.
[63] J.D.K. Donaldson, A. Nicholson, D.G. Southern, J. T., ^{121}Sb Mössbauer studies on Mo_3Sb_7 and $Nb_3Sb_2Te_5$, Acta Chem. Scand. 28a (1975) 866–870.
[64] V.K. Michaelis, S. Kroeker, ^{73}Ge solid-state NMR of germanium oxide materials: experimental and theoretical studies, J. Phys. Chem. C. 114 (2010) 21736–21744.
[65] L. Downward, C.H. Booth, W.W. Lukens, F. Bridges, A variation of the F-test for determining statistical relevance of particular parameters in EXAFS Fits. AIP Conf. Proc. 882 (2007) 129–131.